Available online at www.sciencedirect.com
SCIENCE DIRECT®
ELSEVIER
International Journal of Solids and Structures 43 (2006) 5386–5402
INTERNATIONAL JOURNAL OF SOLIDS and STRUCTURES
www.elsevier.com/locate/ijsolstr

Discussion

Use of magnetorheological elastomer in an adaptive sandwich beam with conductive skins. Part I: Magnetoelastic loads in conductive skins

G.Y. Zhou *, Q. Wang

Department of Mechanical, Materials and Aerospace Engineering, University of Central Florida, Orlando, FL 32816, USA

Received 14 April 2005; received in revised form 28 June 2005
Available online 28 September 2005

Abstract

In this study, the magnetoelastic loads for a vibrating conductive beam exposed perpendicularly to an applied steady magnetic field are addressed analytically by considering the effect of finite dimensions. The dynamic equation of such vibrating beam is presented and a simply supported conductive beam is simulated. The simulation indicates that the magnetoelastic loads affect the dynamic properties of the vibrating beam significantly only when the thickness of the beam is extremely small. This work is the basis for investigating and analyzing the field-controllable dynamic properties of a sandwich beam composed of conductive thin outer skins and a magnetorheological elastomer core, which will be presented in the second part of this research.

Keywords: Magnetoelastic loads; Vibrating beam; Magnetorheological elastomer

1. Introduction

Sandwich beams with magnetorheological elastomer (MRE) cores possess field-controllable flexure rigidities due to the field-dependant shear modulus of the MRE core (Zhou and Wang, 2005). Due to the rapid and reversible change of the flexure rigidity of such beams, they are very potential in developing stiffness controllable devices for semi-active vibration control and flexible structures. Recently, Zhou and Wang reported the field-controllable flexure rigidity of such sandwich beams with non-conductive skins through a high-order beam theory (Zhou and Wang, 2005). The resonant frequencies and anti-resonant

* Corresponding author. Tel.: +1 407 207 7426.
E-mail address: gangyi@gmail.com (G.Y. Zhou).

0020-7683/$ - see front matter © 2005 Elsevier Ltd. All rights reserved.
doi:10.1016/j.ijsolstr.2005.07.042

Nomenclature

$\mathbf{H_0}$	strength of the applied magnetic field
$\mathbf{B_0}$	magnetic induction of the applied magnetic field in free space
T	half-thickness of the conductive beam under consideration
L	half-length of the conductive beam under consideration
$\mathbf{H}$	distribution of magnetic field strength
$\mathbf{B}$	distribution of magnetic induction
$\mathbf{J}$	distribution of current density
$\mathbf{E}$	distribution of electrical field strength
$\mathbf{h}$	disturbance of magnetic field strength
$\mathbf{b}$	disturbance of magnetic induction
$\mathbf{j}$	disturbance of the current distribution
$\mathbf{e}$	disturbance of electrical field strength
$\mathbf{u}$	the displacement field
$\mathbf{v}$	the velocity field
e	longitudinal extension of the conductive beam
w	flexural deflection of the conductive beam
μ_e	magnetic permeability of the electro-conductive media (beam)
μ_r	relative magnetic permeability of the electro-conductive media (beam)
$\mathbf{f^e}$	Lorenz body force in the beam
Π_{pq}	Maxwell's stress tensor
σ_{pq}	stress tensor
ϕ_1 and ϕ_2	potential function associated with the field outside the beam. Subscript "1" means the space up the beam and subscript "2" means the space below the beam
ψ_x	jump of the magnetic field strength along x-direction (fictitious function), see Eq. (13a)
ψ_z	jump of the magnetic field strength along z-direction (fictitious function), see Eq. (13b)
$f_1(x)$	$\mu_r h_z^-(x, T)$ on the upper surface of the beam
$f_2(x)$	$\mu_r h_z^-(x, -T)$ on the lower surface of the beam
x, z	the coordinates of the laboratory frame/absolute frame
i	imaginary unit
$\hat{\mathbf{x}}$ and $\hat{\mathbf{z}}$	the unit vector of x-axis and z-axis of the laboratory frame
"+" and "−"	these subscript means field functions inside the beam (−) or outside the beam (+)
rot	curl operation

Remarks: the italic characteristics associated with the above defined vectors refer to the modulus of the vectors; For example, B_0 is the modulus of $\mathbf{B_0}$.The italic characteristics associated with the above defined vectors and subscribed by the indices of "1, 2, 3" or "x, z" means the component of the vectors. For example, B_{0k} means the k component of $\mathbf{B_0}$ and u_x means the x component of $\mathbf{u}$.

frequencies of such a sandwich beam with non-conductive skins were reported to change up to 30% with applied magnetic fields. To give a systematic study on field-controllable flexure rigidity on such sandwich beams, the case of conductive skins is very important be to investigated, which is the major objective of this research.

For a sandwich beam with an MRE core and two conductive skins, the magnetoelastic loads should be considered in modeling since motion of a conductive skin exposed to a steady magnetic field induces eddy

current and generates an additional unsteady magnetic field. The field disturbance induces Lorenz body forces and surface forces caused by the jump of Maxwell's stress tensor on the surface. Such forces are coupled with the motion of the body. The distribution of the induced-eddy current (Kwon et al., 2003) and the electro-magneto-mechanical coupled problem (Ren and Razek, 1990) were widely addressed in literature. Most of these works were discussed numerically, such as virtual work based edge-element method (Ren and Razek, 1990). Qin et al. (2003) investigated the magnetic loads of a deforming cylindrical shell analytically. In their work, the magnetic field was applied parallel to the axis direction and the effect of finite dimension was considered. As a ramification, they presented the approximation form of the analytical solution for magnetoelastic forces for extra thin vibrating beams exposed parallel to the magnetic field. However, the magnetoelastic forces for a conductive beam exposed perpendicularly to applied steady magnetic fields are still questions unsolved, which are basis for modeling the field-controllable dynamic flexure rigidity of MRE-based sandwich beams with conductive skins. This part of this research is presented to solve this problem to provide analytical solutions of the motion-caused magnetoelastic loads applied to the conductive beam and the effect of the finite dimensions on such loads. A simply supported conductive beam is simulated numerically to show the effect of the magnetoelastic loads.

2. The magneto-mechanical coupling characteristic of a conductive beam

2.1. Problem description

A vibrating conductive beam is exposed to an applied steady magnetic field, which is along z-direction, as shown in Fig. 1. The strength of the magnetic field is $\mathbf{H_0}$ and the corresponding magnetic flux density is denoted by $\mathbf{B_0}$. The thickness and the length of the beam are $2T$ and $2L$, respectively. Because of the motion of the beam, the magnetic eddy-current will be induced such that the applied magnetic field will be disturbed. The field-disturbance will lead to Lorenz body forces and surface forces due to the Maxwell's stress jump on the surface of the beam (Qin et al., 2003). The following analysis is to derive the analytical solution for the Lorenz body force and the surface force due to the motion of the beam when the beam is exposed to the steady magnetic field perpendicularly. The similar procedure and the same basic assumptions as employed in the reference (Qin et al., 2003) will also be adopted in our analysis, except we consider the case of conducive beams placed perpendicular to applied magnetic fields.

2.2. The assumptions

The following basic assumptions are employed.

1. The beam is assumed to be made of perfective conductive material such that the conductivity approaches infinite.

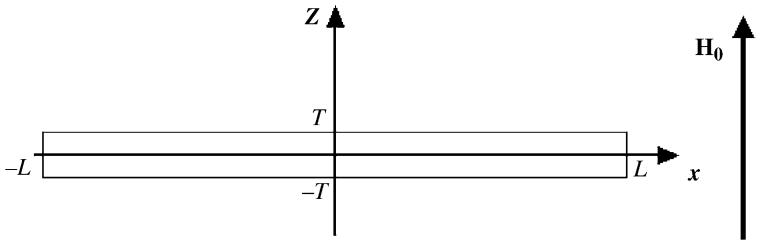

Fig. 1. Illustration of the vibrating beam exposed to the magnetic field perpendicularly.

2. The applied magnetic field is steady and there are no steady electric current and electric field.
3. The induced disturbance of the electro-magnetic field is very small compared with the applied steady magnetic field. Therefore, all the fields in the laboratory frame can be expressed by the following equations:

$$\mathbf{H} = \mathbf{H_0} + \mathbf{h} \tag{1a}$$

$$\mathbf{B} = \mathbf{B_0} + \mathbf{b} \tag{1b}$$

$$\mathbf{J} = \mathbf{0} + \mathbf{j} \tag{1c}$$

$$\mathbf{E} = \mathbf{0} + \mathbf{e} \tag{1d}$$

where **H**, **B**, **J**, **E** are the magnetic field strength, magnetic flux density, current density and the electrical field strength, respectively, and **h**, **b**, **j**, **e** are the induced field intensities whose modulus are much smaller than their undisturbed counterparts.
4. The quasi-static assumption is employed such that the first-order derivative of the displacement current and the electro-magnetic momentum with respect to time can be discarded.
5. The displacement field and the velocity field are denoted by **u**, **v**, respectively. They are functions of spatial coordinate and time. The gradient of **u**, $\nabla\mathbf{u}$, is assumed to be very small such that **v** equals to the partial differential of **u** with respect to time.

2.3. The Lorentz force

Based on the Euler–Bernoulli beam theory, the displacement distribution can be assumed in the following form

$$u_x = e(x,t) - z\frac{\partial w}{\partial x} \tag{2a}$$

$$u_z = w(x,t) \tag{2b}$$

where u_x and u_z is the component of **u**, e and w denote the longitudinal extension and flexural deflection of the beam, respectively.

Under the basic assumptions, the Ohm's law and Faraday's law yield:

$$\mathbf{b}^- = (\mathbf{B_0}\cdot\nabla)\mathbf{u} - \mathbf{B_0}(\nabla\cdot\mathbf{u}) \tag{3}$$

where the superscript "$-$" denotes the quantitative inside the beam. Since the steady magnetic field is applied along z-direction and **u** is a two-dimensional vector function with respect to x- and z-coordinates, the magnetic flux density inside the beam can be further recast into

$$\mathbf{b}^- = -B_0\frac{\partial w}{\partial x}\hat{\mathbf{x}} - B_0\hat{\mathbf{z}}\left(\frac{\partial e}{\partial x} - z\frac{\partial^2 w}{\partial x^2}\right) \tag{4}$$

where $\hat{\mathbf{x}}$ and $\hat{\mathbf{z}}$ are the unit vector of x- and z-coordinates, respectively, B_0 is the modulus of $\mathbf{B_0}$.

Up to the first-order approximation of the induced magnetic field, the Lorenz body force applied to the beam can be expressed as

$$\mathbf{f^e} = \mathbf{J}\times\mathbf{B} = \mathrm{rot}\left(\frac{1}{\mu_e}\mathbf{b}^-\right)\times\mathbf{B_0} = -\frac{1}{\mu_e}\left[\left(\nabla^2\mathbf{u}\right)\times\mathbf{B_0}\right]\times\mathbf{B_0} \tag{5}$$

where μ_e is the magnetic permeability of the beam.

Substitution of Eq. (2) into the above equation yields

$$\mathbf{f}^{\mathbf{e}} = \frac{B_0^2}{\mu_e}\left(\frac{\partial^2 e}{\partial x^2} - z\frac{\partial^3 w}{\partial x^3}\right)\hat{\mathbf{x}} \tag{6}$$

Eq. (6) indicates that the Lorenz body force caused by the vibration of the beam is along x-direction. Thus, this force will induce tensile deformation.

2.4. The surface force due to the Maxwell's stress jump on the surface

From the small disturbance assumption, the stress on the surface of the beam caused by Maxwell's stress jump can be expressed as

$$\sigma_{pq}n_q = \left(\Pi_{qp}^{+} - \Pi_{qp}^{-}\right)n_q = B_{0q}n_q\left[h_p^{+} - \mu_r h_p^{-}\right] - B_{0k}\left[h_k^{+} - \mu_r h_k^{-}\right]n_p, \quad p = x, z \tag{7}$$

where the Einstein's summation convention referred to the repeated indices is adopted; $\mu_r \equiv \mu_e/\mu_0$ is the relative permeability of the beam; the superscript "+" and "−" denote the quantities on the outside and inside of the beam surface, respectively; n_p is the component of the outward normal of the deformed beam surface; Π_{pq} is the Maxwell's stress tensor.

In Eq. (7), the stress on the surface is caused by the discontinuity of the magnetic field strength on the surface of the beam. Considering the applied steady magnetic field is along z-direction, Eq. (7) can be recast into

At $z = T$ or $z = -T$:

$$\begin{cases} \sigma_{zx}^{-} = \left(\Pi_{zx}^{+} - \Pi_{zx}^{-}\right) = B_0\left[h_x^{+} - \mu_r h_x^{-}\right] = B_0\left(h_x^{+} + \frac{B_0}{\mu_0}\frac{\partial w}{\partial x}\right) \\ \sigma_{zz}^{-} = \Pi_{zz}^{+} - \Pi_{zz}^{-} = B_0\left[h_z^{+} - \mu_r h_z^{-}\right] = 0 \end{cases} \tag{8}$$

Thus, it can be seen the surface stress caused by the Maxwell's stress jumps will induce shear deformation of the beam, and will also generate flexural moment distribution on the beam.

From Eqs. (6) and (8), the magnetoelastic loads are completely governed by the motion of the beam and the magnetic field strength outside the beam. Thus, efforts will only be paid on solving $\mathbf{h}^{+}$, the disturbance of the magnetic field strength outside the beam.

3. The disturbance of the magnet field outside the beam

3.1. Governing equations

As stated in the above section, the magnetic field inside the beam is completely determined by the deformation of the beam (see Eq. (4)). Thus, in the analysis of the outside magnetic field, the deformation of the beam is neglected and the problem is recast into solving the magnetic field with the given magnetic boundary condition on the surface of the beam. Under the quasi-static assumption, introduction of two potential functions defined in the upper area and lower area of the beam, respectively, yields:

$$\nabla\phi_1 = \mathbf{h}_1^{+} \quad \text{and} \quad \nabla\phi_2 = \mathbf{h}_2^{+} \tag{9}$$

Thus, the governing equation is Laplace equation as stated below together with the boundary condition.

$$\frac{\partial^2\phi_1}{\partial x^2}+\frac{\partial^2\phi_1}{\partial z^2}=0 \quad \text{for } z>T \quad \text{or } |x|>L \tag{10a}$$

$$\left.\frac{\partial\phi_1}{\partial z}\right|_{z=T}=f_1(x)=\mu_r h_z^-(x,T) \quad \text{for } |x|<L \tag{10b}$$

Similarly, ϕ_2 should satisfy the following equations

$$\frac{\partial^2\phi_2}{\partial x^2}+\frac{\partial^2\phi_2}{\partial z^2}=0 \quad \text{for } z<-T \quad \text{or } |x|>L \tag{11a}$$

$$\left.\frac{\partial\phi_2}{\partial z}\right|_{z=-T}=f_2(x)=\mu_r h_z^-(x,-T) \quad \text{for } |x|<L \tag{11b}$$

It should be pointed out that only the magnetic boundary condition on the upper and lower surface of the beam is considered since their areas are much larger than that of other surfaces of the beam. The tangent component of the magnetic field across the beam surface is discontinuous, which indicates the electrical current will be generated on the surface of the beam in order to satisfy Ampere's law. The compatibility conditions between the potential functions ϕ_1 and ϕ_2 are enforced at $z=0$ when $|x|>L$, which yields

$$\frac{\partial\phi_1}{\partial x}=\frac{\partial\phi_2}{\partial x}, \quad z=0 \quad \text{and} \quad |x|>L \tag{12a}$$

$$\frac{\partial\phi_1}{\partial z}=\frac{\partial\phi_2}{\partial z}, \quad z=0 \quad \text{and} \quad |x|>L \tag{12b}$$

Similar to the method presented in the reference (Qin et al., 2003), two fictitious functions are introduced to lead the explicit solution of the two potential functions as follows:

$$\text{At } z=0\text{:} \quad \frac{\partial\phi_1}{\partial x}-\frac{\partial\phi_2}{\partial x}=\begin{cases}0 & |x|>L\\ \psi_x(x) & |x|<L\end{cases} \tag{13a}$$

and

$$\frac{\partial\phi_1}{\partial z}-\frac{\partial\phi_2}{\partial z}=\begin{cases}0 & |x|>L\\ \psi_z(x) & |x|<L\end{cases} \tag{13b}$$

where $\psi_x(x)$ and $\psi_z(x)$ are the two introduced fictitious functions.

3.2. Solution of the potential functions

The Fourier transform of ϕ_m for $m=1, 2$ with respect to x is defined as

$$\hat{\phi}_m(\omega,z)=\int_{-\infty}^{+\infty}\phi_m(x,z)\exp(-\mathrm{i}\omega x)\,\mathrm{d}x \tag{14}$$

where i is the imaginary unit.

Applying Fourier transform on both sides of Eqs. (10a) and (11a) yields

$$\hat{\phi}_1(\omega,z)=c_1(\omega)\exp(-|\omega|z) \tag{15}$$

$$\hat{\phi}_2(\omega,z)=c_2(\omega)\exp(|\omega|z) \tag{16}$$

where $c_1(\omega)$ and $c_2(\omega)$ are functions to be determined by the boundary condition.

Substituting Eqs. (15) and (16) to Eqs. (12) and (13) yields

$$c_1(\omega) = \frac{1}{\mathrm{i}2\omega}\int_{-L}^{L}\psi_x(x)\exp(-\mathrm{i}\omega x)\,\mathrm{d}x - \frac{1}{2|\omega|}\int_{-L}^{L}\psi_z(x)\exp(-\mathrm{i}\omega x)\,\mathrm{d}x \tag{17a}$$

$$c_2(\omega) = -\frac{1}{2|\omega|}\int_{-L}^{L}\psi_z(x)\exp(-\mathrm{i}\omega x)\,\mathrm{d}x - \frac{1}{\mathrm{i}2\omega}\int_{-L}^{L}\psi_x(x)\exp(-\mathrm{i}\omega x)\,\mathrm{d}x \tag{17b}$$

Thus, the potential function ϕ_1 can be expressed as

$$\begin{aligned}\phi_1(x,z) &= \frac{1}{2\pi}\int_{-\infty}^{+\infty} c_1(\omega)\exp(-|\omega|z)\exp(\mathrm{i}\omega x)\,\mathrm{d}\omega \\ &= \frac{1}{2\pi}\int_{-\infty}^{+\infty}\left[\begin{array}{c}\dfrac{1}{\mathrm{i}2\omega}\displaystyle\int_{-L}^{L}\psi_x(s)\exp(-\mathrm{i}\omega s)\,\mathrm{d}s \\ -\dfrac{1}{2|\omega|}\displaystyle\int_{-L}^{L}\psi_z(s)\exp(-\mathrm{i}\omega s)\,\mathrm{d}s\end{array}\right]\exp(-|\omega|z)\exp(\mathrm{i}\omega x)\,\mathrm{d}\omega \\ &= \left\{\begin{array}{l}\displaystyle\int_{-L}^{L}\psi_x(s)\left[\int_0^{+\infty}\frac{\exp(-\omega z)\sin(\omega(x-s))}{2\pi\omega}\,\mathrm{d}\omega\right]\mathrm{d}s \\ \displaystyle-\int_{-L}^{L}\psi_z(s)\left[\int_0^{+\infty}\frac{\exp(-\omega z)\cos(\omega(x-s))}{2\pi\omega}\,\mathrm{d}\omega\right]\mathrm{d}s\end{array}\right\}\end{aligned} \tag{18}$$

The following identities can be used for Eq. (18):

$$\int_0^{+\infty}\frac{\exp(-a\omega)\sin(b\omega)}{\omega}\,\mathrm{d}\omega = \operatorname{arc\,cot}\left(\frac{a}{b}\right) \tag{19a}$$

$$\int_0^{+\infty}\frac{\exp(-\omega a)\cos(\omega b)}{\omega}\,\mathrm{d}\omega = -\frac{1}{2}\ln\left(a^2+b^2\right) \tag{19b}$$

Thus, Eq. (18) can be recast into

$$\phi_1(x,z) = \frac{1}{2\pi}\int_{-L}^{L}\psi_x(s)\operatorname{arc\,cot}\left(\frac{z}{x-s}\right)\mathrm{d}s + \frac{1}{4\pi}\int_{-L}^{L}\psi_z(s)\ln\left(z^2+(x-s)^2\right)\mathrm{d}s \tag{20}$$

Similarly, the potential function ϕ_2 can be expressed as

$$\phi_2(x,z) = \frac{1}{2\pi}\int_{-L}^{L}\psi_x(s)\operatorname{arc\,cot}\left(\frac{z}{x-s}\right)\mathrm{d}s + \frac{1}{4\pi}\int_{-L}^{L}\psi_z(s)\ln\left(z^2+(x-s)^2\right)\mathrm{d}s \tag{21}$$

Substituting the boundary conditions, Eqs. (10b) and (11b), to Eqs. (20) and (21), the fictitious functions $\psi_x(x)$ and $\psi_z(x)$ can be identified:

$$-\int_{-L}^{L}\psi_x(s)\frac{x-s}{T^2+(x-s)^2}\,\mathrm{d}s + \int_{-L}^{L}\psi_z(s)\frac{T}{T^2+(x-s)^2}\,\mathrm{d}s = 2\pi f_1(x) \tag{22a}$$

$$-\int_{-L}^{L}\psi_x(s)\frac{x-s}{T^2+(x-s)^2}\,\mathrm{d}s - \int_{-L}^{L}\psi_z(s)\frac{T}{T^2+(x-s)^2}\,\mathrm{d}s = 2\pi f_2(x) \tag{22b}$$

Thus, $\psi_x(x)$ and $\psi_z(x)$ can be solved by the following two integral equations.

$$\int_{-L}^{L}\psi_x(s)\frac{x-s}{T^2+(x-s)^2}\,\mathrm{d}s = -\pi[f_1(x)+f_2(x)] \tag{23a}$$

$$\int_{-L}^{L}\psi_z(s)\frac{T}{T^2+(x-s)^2}\,\mathrm{d}s = \pi[f_1(x)-f_2(x)] \tag{23b}$$

Once $\psi_x(x)$ and $\psi_z(x)$ is obtained, the potential functions can be obtained though Eqs. (20), and (21) consequently.

An interesting phenomenon in Eq. (23) deserves our special attention. If $f_1(x)$ and $f_2(x)$ are equal, we have $\psi_z(x) = 0$; if $f_1(x)$ and $f_2(x)$ are opposite, we have $\psi_x(x) = 0$. This phenomena is held no matter what the thickness of the beam is. Thus, when the thickness of the beam approaches zero, it is doubtful to assume $f_1(x) = f_2(x)$ or $f_1(x) = -f_2(x)$ only because the thickness is negligible, which was employed in the reference (Qin et al., 2003). In the following, we will use the phenomenon revealed by Eq. (23) in our analysis of the special case of extra thin beams.

A summary to the whole solution process is given as follows. First, the magnetic field inside the conductive skin can be easily obtained once the deformation of the beam is given. And, as a result, the boundary conditions of $f_1(x)$ and $f_2(x)$ are also yielded. Secondly, the fictitious functions $\psi_x(x)$ and $\psi_z(x)$ can be determined through Eqs. (23a) and (23b) considering the boundary condition. Thirdly, the solutions of induced magnetic potentials are determined by substituting the solutions of $\psi_x(x)$ and $\psi_z(x)$ into Eqs. (20) and (21).

From the obtained potential function, the magnetic field strength is

$$h_{1x}^{+} = h_{2x}^{+} = \frac{\partial \phi_1(x,z)}{\partial x} = \frac{\partial \phi_2(x,z)}{\partial x} = \frac{1}{2\pi}\int_{-L}^{L} \psi_x(s) \frac{z}{(x-s)^2 + z^2}\,\mathrm{d}s + \frac{1}{2\pi}\int_{-L}^{L} \psi_z(s) \frac{x-s}{z^2 + (x-s)^2}\,\mathrm{d}s \tag{24a}$$

$$h_{1z}^{+} = h_{2z}^{+} = \frac{\partial \phi_1(x,z)}{\partial z} = \frac{\partial \phi_2(x,z)}{\partial z} = -\frac{1}{2\pi}\int_{-L}^{L} \psi_x(s) \frac{x-s}{(x-s)^2 + z^2}\,\mathrm{d}s + \frac{1}{2\pi}\int_{-L}^{L} \psi_z(s) \frac{z}{z^2 + (x-s)^2}\,\mathrm{d}s \tag{24b}$$

4. The field-disturbance and the magnetoelastic loads for extra thin beams

In this section, the case of extra thin beams exposed to magnetic field perpendicularly will be investigated analytically. The stress due to Maxwell's stress jump on the surface and the characteristics of the disturbance field due to the motion-induced eddy current on the conductive beams are two main issues for this section.

4.1. The fictitious functions ψ_x and ψ_z for extra thin beams

From Eq. (4), $f_1(x)$ and $f_2(x)$ can be expressed as

$$f_1(x) = -\frac{B_0}{\mu_0}\left(\frac{\partial e}{\partial x} - T\frac{\partial^2 w}{\partial x^2}\right) \tag{25a}$$

$$f_2(x) = -\frac{B_0}{\mu_0}\left(\frac{\partial e}{\partial x} + T\frac{\partial^2 w}{\partial x^2}\right) \tag{25b}$$

Thus, the following relationships are valid

$$f_1(x) + f_2(x) = -\frac{B_0}{\mu_0}\frac{\partial e}{\partial x} \tag{26a}$$

$$f_1(x) - f_2(x) = -2\frac{B_0 T}{\mu_0}\frac{\partial^2 w}{\partial x^2} \tag{26b}$$

From the above equation and Eq. (23), it can be seen $\psi_x(x)$ depends on the longitudinal displacement of the beam while $\psi_z(x)$ relies on the flexure deflection. Since the longitudinal displacement is associated with the Young's modulus of the beam, which is much larger than flexure rigidity of extra thin beams, the longitudinal displacement can be neglected. Thus, we have $f_1(x) = -f_2(x)$ and $f_1(x) = -\frac{B_0 T}{\mu_0}\frac{\partial^2 w}{\partial x^2}$.

For the case of thin beam, $\frac{T}{L}$ is assumed to approach zero. According to Appendix B, Eq. (23) can be expressed as

$$\begin{aligned}\lim_{\widetilde{T}\to 0}\int_{-L}^{L}\psi_x(s)\frac{x-s}{T^2+(x-s)^2}\,\mathrm{d}s &= \lim_{\widetilde{T}\to 0}\int_{-1}^{1}\psi_x(\tilde{s}L)\frac{\tilde{x}-\tilde{s}}{\widetilde{T}^2+(\tilde{x}-\tilde{s})^2}\,\mathrm{d}\tilde{s} = \psi_x(x)\ln\left|\frac{x+L}{x-L}\right| \\ &= -\pi[f_1(x)+f_2(x)] \end{aligned} \tag{27}$$

Thus, it yields

$$\psi_x(x) = \frac{-\pi[f_1(x)+f_2(x)]}{\ln\left|\frac{x+L}{x-L}\right|} \tag{28}$$

Similarly, according to Appendix A, the solution for $\int_{-L}^{L}\psi_z(s)\frac{T}{T^2+(x-s)^2}\,\mathrm{d}s = \pi[f_1(x)-f_2(x)]$ is

$$\psi_z(x) = \begin{cases} f_1(x)-f_2(x) & -L<x<L \\ 0 & x>L \text{ or } x<-L \\ \frac{f_1(x)-f_2(x)}{2} & x=L \text{ or } x=-L \end{cases} \tag{29}$$

4.2. The stress due to Maxwell's stress jumps on the surface of extra thin beams

From Eqs. (24), (26) and (27), the strength of the magnetic field at the outer surface of the thin beam can be expressed as

$$\lim_{T/L\to 0} h_{1x}^{+}(z=T) = -\frac{1}{2}\frac{\pi[f_1(x)+f_2(x)]}{\ln\left|\frac{x+L}{x-L}\right|} + \frac{f_1(x)-f_2(x)}{2\pi}\ln\left|\frac{x+L}{x-L}\right| \tag{30a}$$

$$\lim_{T/L\to 0} h_{2x}^{+}(z=-T) = \frac{1}{2}\frac{\pi[f_1(x)+f_2(x)]}{\ln\left|\frac{x+L}{x-L}\right|} + \frac{f_1(x)-f_2(x)}{2\pi}\ln\left|\frac{x+L}{x-L}\right| \tag{30b}$$

$$\lim_{T/L\to 0} h_{1z}^{+}(z=T) = f_1(x) \tag{30c}$$

$$\lim_{T/L\to 0} h_{2z}^{+}(z=-T) = f_2(x) \tag{30d}$$

From Eq. (8) and substituting the expression of $f_1(x)$ and $f_2(x)$ solved by Eq. (26), the Maxwell's stress jump on the surface for this special case can be expressed

$$\sigma_{zx} = \frac{B_0^2}{\mu_0}\left(\frac{\pi}{2\ln\left|\frac{x+L}{x-L}\right|}\frac{\partial e}{\partial x} - \frac{T}{\pi}\frac{\partial^2 w}{\partial x^2}\ln\left|\frac{x+L}{x-L}\right| + \frac{\partial w}{\partial x}\right) \tag{31}$$

4.3. Characteristics of the field-disturbance due to the motion-induced eddy current

We have concluded that $f_1(x) = -f_2(x)$ is reasonable for thin beams. Thus, by Eqs. (23) and (24), the strength of the field-disturbance, **h**, outside the thin beam follows the following inequalities:

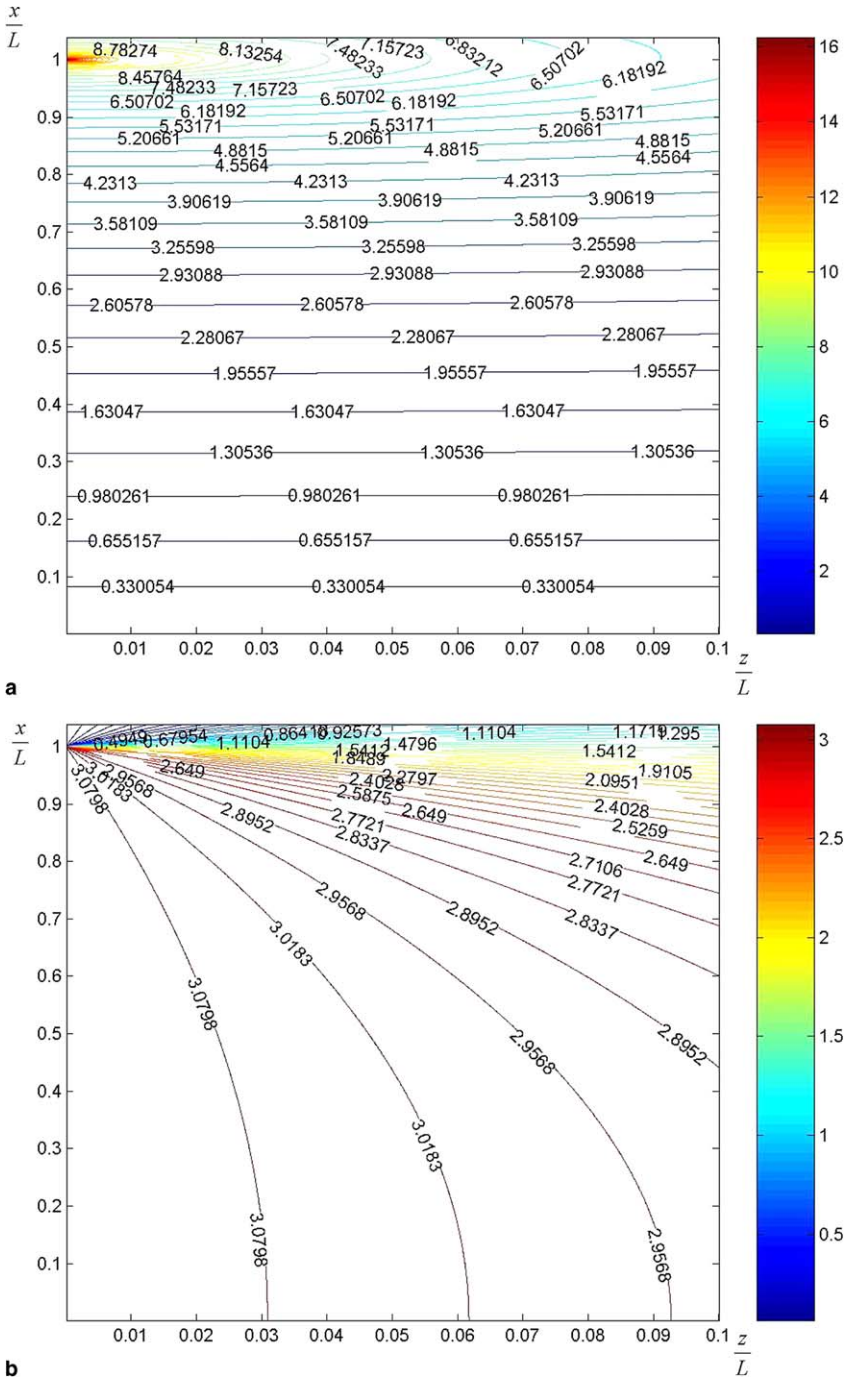

Fig. 2. Pattern of the field-disturbance due to motion induced eddy current on thin conductive beams.

$$\left|h_{1x}^{+}\right| = \left|h_{2x}^{+}\right| = \left|\frac{1}{2\pi}\int_{-L}^{L}\psi_z(s)\frac{x-s}{z^2+(x-s)^2}\,\mathrm{d}s\right| \leqslant \frac{1}{2\pi}\left|\int_{-L}^{L}\psi_z(s)\,\mathrm{d}s\right|\left|\int_{-L}^{L}\frac{x-s}{z^2+(x-s)^2}\,\mathrm{d}s\right|$$
$$= \frac{1}{2\pi}\left|\int_{-L}^{L}\psi_z(s)\,\mathrm{d}s\right|\left|\ln\frac{z^2+(L-x)^2}{z^2+(L+x)^2}\right| \tag{32a}$$

$$\left|h_{1z}^{+}\right| = \left|h_{2z}^{+}\right| = \frac{1}{2\pi}\left|\int_{-L}^{L}\psi_z(s)\frac{z}{z^2+(x-s)^2}\,\mathrm{d}s\right|$$
$$\leqslant \frac{1}{2\pi}\left|\int_{-L}^{L}\psi_z(s)\,\mathrm{d}s\right|\left|\arctan\frac{L-x}{z}+\arctan\frac{L+x}{z}\right| \tag{32b}$$

From the above two equations, we can see the functions of $\left|\ln\frac{z^2+(L-x)^2}{z^2+(L+x)^2}\right|$ and $\left|\arctan\frac{L-x}{z}+\arctan\frac{L+x}{z}\right|$ determines the pattern of the x component and z component of the field-disturbance outside the conductive thin beam, respectively. Fig. 2 illustrated the contours of these two functions against z/L and x/L. In Fig. 2(a), the x component of **h** outside the beam reaches a sharp peak at the ends of the beam and decays dramatically while the location deviates from the ends of the beam. In Fig. 2(b), the z component of **h** outside the beam is concentrated in the narrow region of $-L\leqslant x\leqslant L$ and decreases when $|x|$ or $|z|$ become larger.

It should be stressed, due to the assumption of small disturbance, the modulus of **h** is extremely small compared with that of $\mathbf{H_0}$. This remark would be very useful in modeling MRE-based sandwich beams with conductive skins, which is the main issue of the other part of the issue. Because it indicates the field disturbance near the two skins of MRE-based sandwich beams with conductive skins can be solved separately as if they are immersed in applied steady magnetic fields solely.

5. Simulations on a simply supported beam

5.1. The governing equation of a vibrating beam

Pure bending is considered in the following simulations. An infinitesimal element of the beam is shown in Fig. 3. The Maxwell's stress jump will induce the shear force σ_{zx} on the upper and lower surface; the shear force at the left and right surface are denoted as Q and $Q+\frac{\partial Q}{\partial x}\,\mathrm{d}x$, respectively; the flexure moment at the left and right surface are denoted as M and $M+\frac{\partial M}{\partial x}\,\mathrm{d}x$; the Lorenz body force will also induce a moment, which is denote as M_{L}; the vertical force acting on the beam is denoted as $q(x,t)$. By Newton's second law, the dynamic equation of this part is

$$\rho A\frac{\partial^2 w}{\partial t^2}\,\mathrm{d}x = -\frac{\partial Q}{\partial x}\,\mathrm{d}x - q(x,t)\,\mathrm{d}x \tag{33}$$

Neglecting the inertial moment effect, the resultant moment applied to the tiny part should be zero. Thus, up to the first-order approximation, the equilibrium equation is

$$-Q\,\mathrm{d}x + \frac{\partial M}{\partial x}\,\mathrm{d}x - M_{\mathrm{L}} - \sigma_{zx}A\,\mathrm{d}x = 0 \tag{34}$$

where A is the cross-section of the beam.

From Eq. (6), M_{L} satisfies the following equation

$$M_{\mathrm{L}} = -\mathrm{d}xH\int_{-T}^{T}z^2\frac{B_0^2}{\mu_{\mathrm{e}}}\frac{\partial^3 w}{\partial x^3}\,\mathrm{d}z = -\mathrm{d}x\frac{T^2B_0^2}{3\mu_{\mathrm{e}}}\frac{\partial^3 w}{\partial x^3}A \tag{35}$$

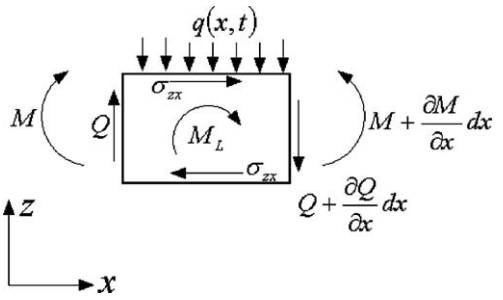

Fig. 3. Force diagram of the beam exposed to magnetic field perpendicularly.

Thus, substituting Eqs. (29) and (35) into Eq. (34) yields

$$\rho A\frac{\partial^2 w}{\partial t^2}+\left(EI+\frac{B_0^2At^2}{3\mu_e}\right)\frac{\partial^4 w}{\partial x^4}+A\frac{B_0^2}{\mu_0}\frac{T}{\pi}\frac{\partial^3 w}{\partial x^3}\ln\left(\frac{L+x}{L-x}\right)+A\frac{B_0^2}{\mu_0}\left(\frac{2LT}{\pi(L^2-x^2)}-1\right)\frac{\partial^2 w}{\partial x^2}=-q(x,t) \tag{36}$$

where EI is the flexure rigidity of the beam.

The governing equation for a beam exposed to an applied magnetic perpendicularly is hence derived.

5.2. The boundary conditions of the simply supported beam

At the two ends of the beam, the vertical displacements are assumed to be zero, which yields

$$w(-L)=w(L)=0 \tag{37}$$

The flexural torque at the two ends should be balanced by the moments induced by magnetoelastic loads. Thus, from Eqs. (6) and (31), the boundary condition at the two ends is

$$\left(1+\frac{3B_0^2}{\mu_0\pi ET}\ln\frac{x+L}{L-x}\right)\frac{\partial^2 w}{\partial x^2}=\frac{3B_0^2}{\mu_0 ET^2}\frac{\partial w}{\partial x}-\frac{B_0^2}{\mu_e E}\frac{\partial^3 w}{\partial x^3} \tag{38}$$

Because $\ln\frac{x+L}{L-x}$ will goes toward infinite as x approaches $-L$ or L. The following conditions must be enforced to satisfy the above equation:

$$\left.\frac{\partial^2 w}{\partial x^2}\right|_{x=-L}=0 \tag{39a}$$

and

$$\left.\frac{\partial^2 w}{\partial x^2}\right|_{x=L}=0 \tag{39b}$$

Therefore, the governing equation of the beam shown in Eq. (36) can be solved by Galerkin method through the basis of $\left\{\sin\left(\frac{k\pi}{2L}x-\frac{k\pi}{2}\right)\middle|k=1,2,3,\ldots\right\}$ by considering the boundary condition of Eqs. (38) and (39).

5.3. Simulation results

In the numerical simulation, the dimensions and material properties of the beam are given as follows. The width of the beam, w_b, is set to be $0.2L$ (1/10 of the length of the beam); the length of the beam, $2L$, is 100 mm; the beam is made of aluminum whose Young's modulus E_t is 72 GPa and the density is

2700 kg/m^3; the relative permeability of the beam, μ_r, is set to be 10. The external harmonic force is applied at the center of the beam with the amplitude of 1 N. The field-induced change of the amplitude of the displacement at the center of the beam, where the external mechanical force is applied, is used in the simulation to reveal the effect of the magnetic field on the vibration of the beam.

The thickness of the beam, $2T$, is set to be 0.5 mm. The amplitude of the displacement at the center of the beam against the frequency of the external force at different magnetic field strengths is given in Fig. 4. From the figure, the displacement at the center of the beam, $|w(0)|$, changes with the induction of the applied magnetic field especially in the low frequency range which is at left of the first resonant frequency. In this low frequency range, the displacement decreases with the applied magnetic field indicating the stiffness of the beam increases with the applied magnetic field. The observation is reasonable since the induced eddy current will prevent the motion of the beam (Faraday's law). The resonant frequencies and the anti-resonant frequencies decrease with the applied magnetic field, also indicating the stiffness of the beam increases with the applied magnetic field. The induced surface forces by the Maxwell's stress jump on the surface of the beam at the first resonant frequency $\left(\frac{\omega}{2\pi} = 146 \text{ Hz}\right)$ is given in Fig. 5 while the corresponding Lorenz body force at the upper surface of the beam ($z = T$) is given in Fig. 6. The two curves are much like and are anti-symmetric around $x = 0$, the center of the beam. The maximum value occurs at the ends of the beam, which indicates the induced eddy current achieves maximum value of the ends. From Faraday's law, this observation reveals that the change of the magnetic flux at the ends of is greater than that of other parts of the beam while, at the center of the beam, the magnetic flux remains constant during the vibration of the beam. The above conclusions on the distribution of the induced eddy current from the calculated magnetoelastic loads can be verified by the following. From Eq. (30a), the induced electrical current density $\mathbf{J_s}$ on the conductive beam can be determined by the Ampere's law:

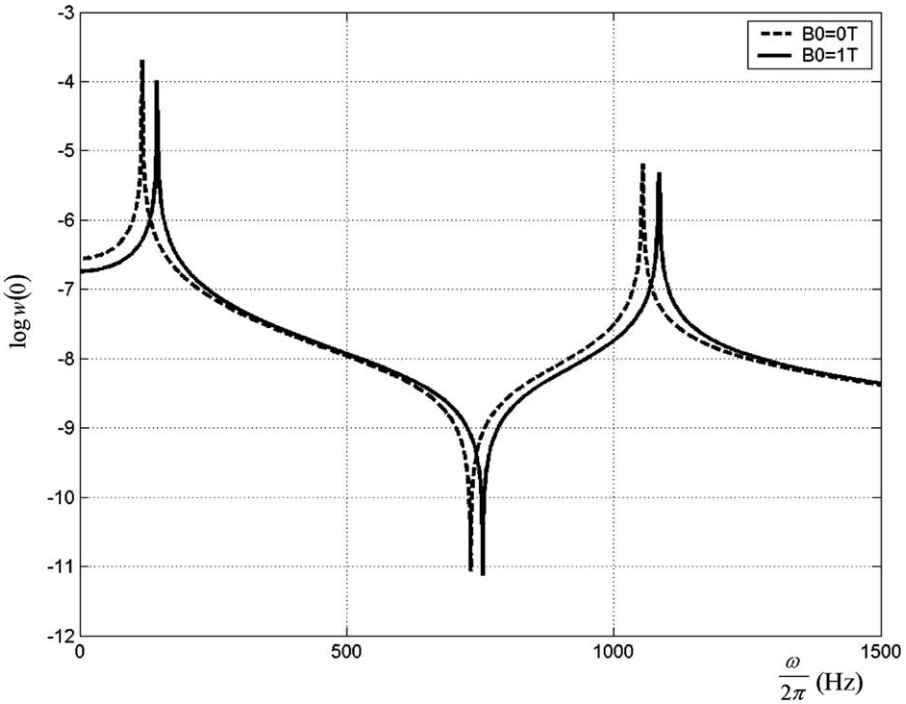

Fig. 4. The amplitude of the displacement at the center of the beam at different magnetic field strengths for the beam with $T = 0.25$ mm.

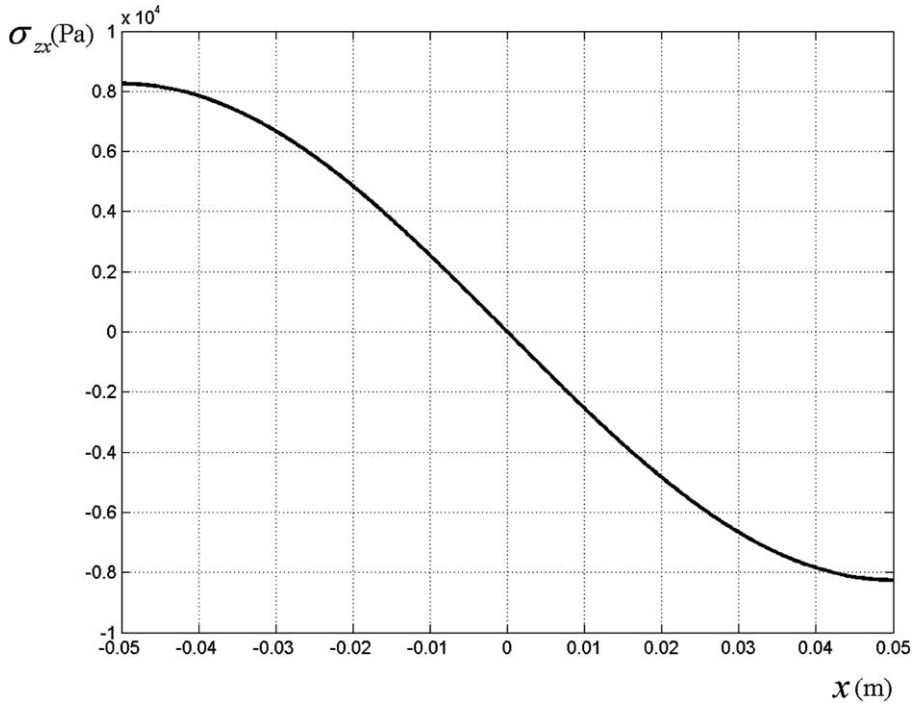

Fig. 5. The surface shear stress induced by the Maxwell stress jumps at the surface for the beam with $T = 0.25$ mm and $B_0 = 1$ T.

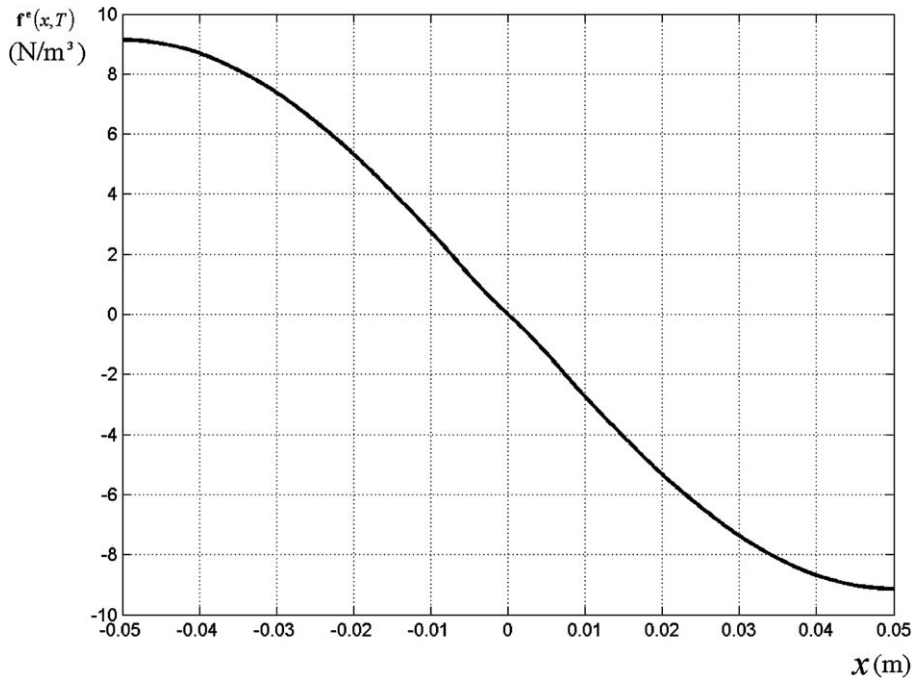

Fig. 6. The Lorenz body force at the upper surface of the beam with $T = 0.25$ mm and $B_0 = 1$ T.

$$\mathbf{J_s} = \left(h_x^+ - h_x^-\right)(\hat{\mathbf{x}} \times \hat{\mathbf{z}}) = \left[-\frac{B_0 T}{\mu_0 \pi} \ln\left(\frac{L+x}{L-x}\right) \frac{\partial^2 w}{\partial x^2} + \frac{B_0}{\mu_e} \frac{\partial w}{\partial x}\right](\hat{\mathbf{x}} \times \hat{\mathbf{z}}) \tag{39}$$

From the obtained deflection of the beam, w, $\mathbf{J_s}$ can be obtained easily from the above equation, which is shown in Fig. 7. The curve is anti-symmetric around the center of the beam, which indicates $\mathbf{J_s}$ is dominated by the second term in the square bracket of the above equation or the first-order derivative of w with respect to x. The current density, $\mathbf{J_s}$, is very large at the ends of the beam and the average electrical current in the left half and the right half of the beam is 26 A. Because the beam is assumed to be perfectly electro-conductive, the electrical resistivity of the beam is zero in the modeling. This is an ideal case since, by Ohm's law, there will be no heat generated. However, in reality, the induced eddy current will generate heat due to the electrical resistance of the beam. This procedure will convert mechanical energy to thermal energy. For example, employing the average electrical current of 26 A and if the electrical resistance of half-beam is lower as 0.01 Ω, the generated heat on the beam would be 13.5 W. As a result, the damping ratio of the beam will increase with the applied magnetic field. Hence, the bandwidth of the displacement curve around the resonant frequencies will increase and the amplitude of the displacement at the resonant frequencies will decrease.

From the Ampere's law, the induced current density inside the beam is

$$\mathbf{j} = \mathrm{rot}\,\mathbf{h}^- = z \frac{\partial^3 w}{\partial x^3} \frac{B_0}{\mu_e} (\hat{\mathbf{x}} \times \hat{\mathbf{z}}) \tag{40}$$

Thus, the induced current density inside the beam is proportional to the Lorenz body force. And, therefore, $\mathbf{j}$ exhibits the same characteristics of those in Fig. 6.

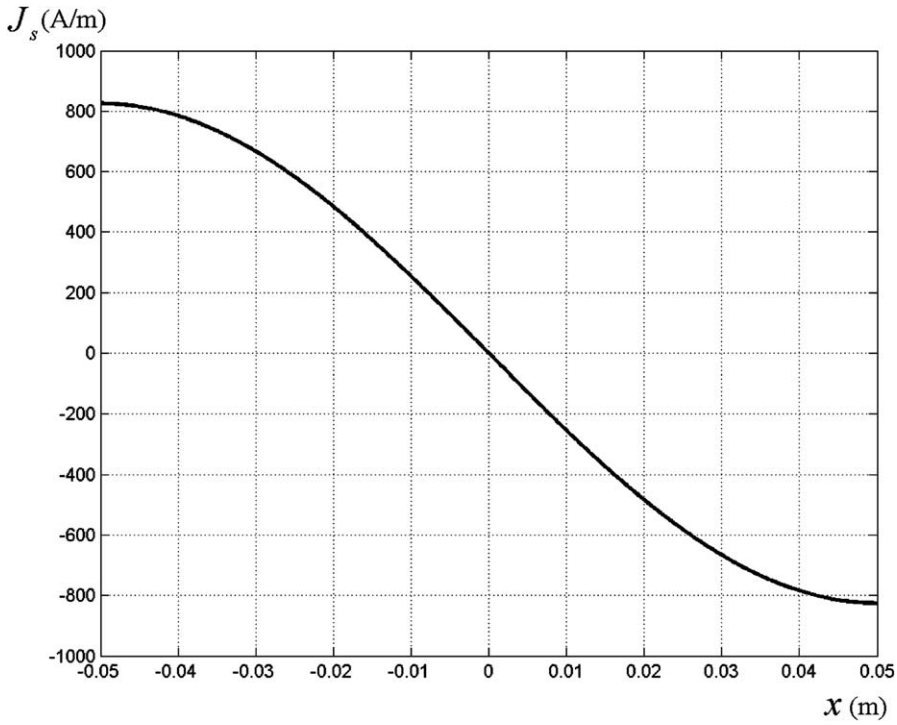

Fig. 7. The density of the electrical current on the upper surface of the beam with $T = 0.25$ mm and $B_0 = 1$ T.

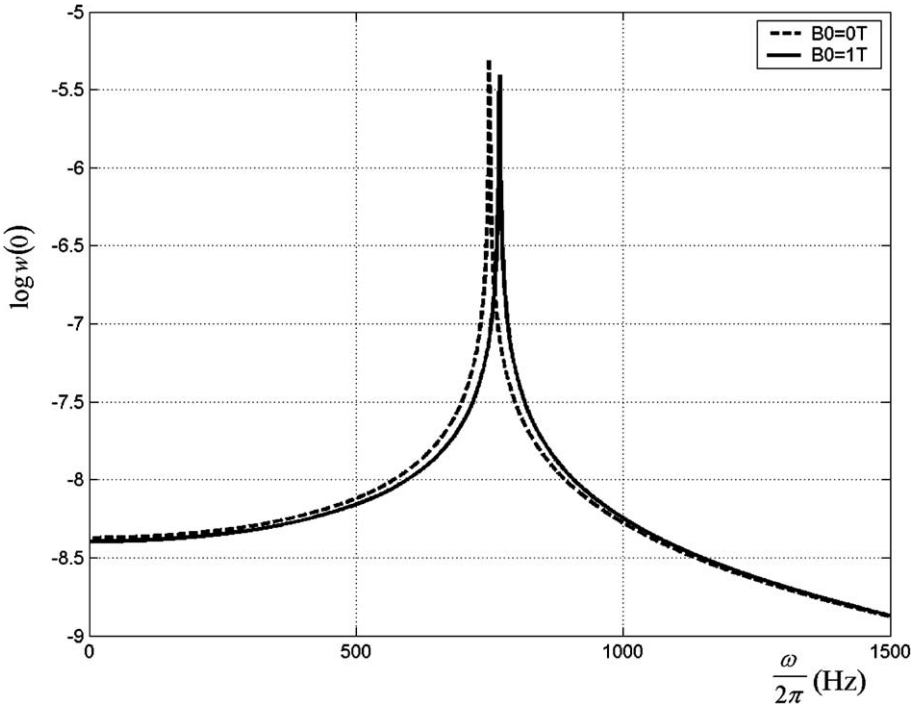

Fig. 8. The amplitude of the displacement at the center of the beam at different magnetic field strengths for the beam with $T = 0.4$ mm.

In the above simulation, the thickness-length ratio of the beam is lower as 0.005. Thus, the beam under simulation is extremely thin. It should be pointed out that the effect of the above magnetic-mechanical coupling phenomenon is affected by the thickness of the beam. In the following simulation, the thickness of the beam, $2T$, is set to be 0.8 mm. The amplitude of the displacement at the center of the beam against the frequency of the external at different magnetic field strengths is given in Fig. 8. From the figure, it can be seen the change of the displacement curves is very small even though the induction of the applied magnetic field is 1 T.

6. Conclusions

The investigation on the magnetoelastic loads subjected to conductive beam perpendicular to the magnetic field is presented in the paper. The Lorenz body force and the magnetic field inside the in the conductive beam can be calculated by the deformation of the beam directly. The surface force caused by the Maxwell's stress jump is related to the magnetic field outside the beam. By the analytical solution of the above surface force and the Lorenz body force, the dynamic equation of a vibrating beam exposed to the applied magnetic field perpendicularly is presented and a vibrating simply supported beam is simulated as an example. Based on the study, the magnetoelastic loads affect the dynamic property of the vibrating beam significantly when the thickness of the beam is small, especially around the resonant frequencies. This study will present a foundation in analyzing the magnetic energy for deriving the governing equation of the MRE-based sandwich beam with conductive skins through the principle of virtual work, which will be presented in the second part of this research.

Appendix A

The limitation of the function $g(\tilde{x},\tilde{z}) = \int_{-1}^{1} f(\tilde{s}) \frac{\tilde{z}}{(\tilde{x}-\tilde{s})^2+\tilde{z}^2}\,\mathrm{d}s$ as $\tilde{z}$ approaches zero will be analyzed in this appendix. This function can be rewritten into the following form:

$$g(\tilde{x},\tilde{z}) = \int_{\frac{\tilde{x}-1}{\tilde{z}}}^{\frac{\tilde{x}+1}{\tilde{z}}} \frac{f(\tilde{x}-s_1\tilde{z})}{1+s_1^2}\,\mathrm{d}s_1 \tag{A.1}$$

As $\tilde{z}$ approaches zero, the following limitation is valid:

$$\lim_{\tilde{z}\to 0} g(\tilde{x},\tilde{z}) = f(\tilde{x}) \lim_{\tilde{z}\to 0}\left[\arctan\left(\frac{\tilde{x}+1}{\tilde{z}}\right) - \arctan\left(\frac{\tilde{x}-1}{\tilde{z}}\right)\right] = \begin{cases} \pi f(\tilde{x}) & -1<\tilde{x}<1 \\ 0 & \tilde{x}>1 \text{ or } \tilde{x}<-1 \\ \frac{\pi f(\tilde{x})}{2} & \tilde{x}=1 \text{ or } \tilde{x}=-1 \end{cases} \tag{A.2}$$

Appendix B

The limitation of the function $g(\tilde{x},\tilde{z}) = \int_{-1}^{1} f(\tilde{s}) \frac{\tilde{x}-\tilde{s}}{(\tilde{x}-\tilde{s})^2+\tilde{z}^2}\,\mathrm{d}s$ as $\tilde{z}$ approaches zero will be analyzed in this appendix. This function can be rewritten into the following form:

$$g(\tilde{x},\tilde{z}) = \int_{\frac{\tilde{x}-1}{\tilde{z}}}^{\frac{\tilde{x}+1}{\tilde{z}}} f(\tilde{x}-\tilde{s}\tilde{z}) \frac{\tilde{s}}{\tilde{s}^2+1}\,\mathrm{d}\tilde{s} \tag{B.1}$$

As $\tilde{z}$ approaches zero, the following limitation is valid

$$\lim_{\tilde{z}\to 0} g(\tilde{x},\tilde{z}) = \frac{f(\tilde{x})}{2} \lim_{\tilde{z}\to 0}\left[\frac{\ln\left[\left(\frac{\tilde{x}+1}{\tilde{z}}\right)^2+1\right]}{\ln\left[\left(\frac{\tilde{x}-1}{\tilde{z}}\right)^2+1\right]}\right] = f(\tilde{x}) \ln\left|\frac{\tilde{x}+1}{\tilde{x}-1}\right| \tag{B.2}$$

References

Kwon, O., Chari, M.V.K., et al., 2003. Development of integral equation solution for 3-D eddy current distribution in a conducting body. IEEE Trans. Magn. 39 (5), 2612–2614.

Qin, Z., Librescu, L., et al., 2003. Magnetoelastic modeling of circular cylindrical shells immersed in a magnetic field. Part I: magnetoelastic loads considering finite dimensional effects. Int. J. Eng. Sci. 41, 2005–2022.

Ren, Z., Razek, A., 1990. A coupled electromagnetic-mechanical model for thin conductive plate deflection analysis. IEEE Trans. Magn. 26 (5), 1650–1652.

Zhou, G.Y., Wang, Q., 2005. Magnetorheological elastomer-based smart sandwich beams with nonconductive skins. Smart Mater. Struct. 14, 1001–1009.